iConclusions https://iconclusions.com/ Conclusions in Engineering

On the Steadfastness of the Least-Square Reverse-Time Migration Wavefield Extrapolation via 1st-Order Riemannian Axis Finite-Difference Solver

Hussein Muhammed,[1,2,3,a)] Xiaodong Sun,[1] Liping Gao,[4] AbdelHafiz Gadelmula,[3] and Zhenchun Li[1]

[1)] *Shandong Provincial Key Laboratory of Reservoir Geology, China University of Petroleum (East China), Qingdao, 266580, China*

[2)] *Xian Key Laboratory of Scientific Computation and Optimization, School of Mathematics and Statistics, Northwestern Polytechnical University, Xi'an, 710072, China*

[3)] *Centre for Seismological Phenomena, Department of Geology, Faculty of Science, University of Khartoum, Sudan*

[4)] *College of Sciences and Arts, School of Mathematics, China University of Petroleum (East China), Qingdao, 266580, China*

ABSTRACT: Exploring Earth's deep regions through pioneering Least-Squares Reverse-Time Migration (LSRTM) methods is of significant interest due to its exceptional structural clarity. This cutting-edge seismic imaging technique is time-consuming and memoryintensive, so wavefield extrapolation is proposed in the Pseudodepth domain (1st-order Riemannian coordinate system's axis) to address these issues and prevent oversampling/aliasing when modeling deeper subsurface zones. Stabilizing the generated Riemannian wavefield involves implementing an appropriate mapping velocity and obtaining the vertical axis operator that partially converts the finite difference solver from time to frequency domains. Each Cartesian point (x, y, z) has a corresponding vertical-time point (ξ_1, ξ_2, ξ_3), allowing interpolation of the reconstructed source wavefield through a Cartesian-to-Riemannian mapping function. Our stability and convergence analysis indicates that the spatial derivatives of the 1^{st} -order Riemannian axis can be approximated by Fourier pseudo-spectral methods and fast-Fourier transforms using a special Gaussian-like impulse function. This function generates the source term vector-matrix within the finite-difference operator. The mapping velocity, derived as a differential form of the initial input velocity model, controls the CFL conditions of the associated Riemannian-finite difference operator. Numerical, synthetic, and seismic field data examples show that this approach is more stable and efficient in extrapolating a smooth 1st-order Riemannian axis-based finitedifference wavefield while adhering to Claerbout's principle for locating subsurface reflectors. Additionally, choosing the appropriate sampling rate for the new vertical axis is inversely related to the maximum frequency of the impulse wavelet and directly related to the minimum velocity value in the model.

Received: 26 Feb. 2025
Accepted: 17 March 2026
DOI: https://doi.org/10.71107/dh3px571

I. INTRODUCTION

The seismic trace contains valuable information that can be associated with changes in rock properties but can be easily masked after an improper processing or modelling workflow. It is shown that all wavefield extrapolation methods are based on two equations; the Taylor series and the specific wave equation; hence all errors are inherited from these formulae. The powerful method of separation of variables can also be applied to the acoustic wave equation in the same way as for the heat and diffusion equations. We know that the size of the associated errors is from the Taylor formula, in addition, there is a magnification of the errors due to the method itself. Migration aims to determine a model of reflectors; however, wave equations do not include such a model parameter representing the reflectors explicitly. Thus, it is necessary to re-parameterize the wave equation for

[a)] Electronic mail: mhmd_hussein@s.upc.edu.cn

incorporating this parameter into the forward modelling formulas for tau-domain wavefield migrations.

The field of seismic data processing has undergone a significant transformation thanks to advancements in theoretical physics and computational mathematics. This progress, driven by enhanced computing capabilities and sophisticated numerical modeling techniques[1,2], has solidified Reverse-Time Migration (RTM) as a robust migration algorithm for industrial use[3–5]. Despite its maturity, RTM involves the backward propagation of recorded data using the adjoint operator of its forward modeling process. Additionally, the zero-lag cross-correlation imaging condition, first proposed by Claerbout (1971) and Claerbout and Doherty (1972), is predominantly employed in RTM over the deconvolution imaging condition. This is because the zero-lag cross-correlation imaging condition is unconditionally stable, and more convenient for the implementation[6]. These two constraints, which are the adjoint-operator and the zero-lag cross-correlation imaging condition, have an impact on the Reverse-Time Migration imaging, decreasing the resolution and amplitude accuracy of the yielded image. To mitigate the limitations as well as keeping the enhanced features of RTM, LSRTM had been introduced[7,8]. The Born approximation represents the property of the reflectors with impedance perturbation while the Kirchhoff approximation describes the property with reflectivity, and the forward modelling formulas based on both approximations include the angles of wave propagation[1,9–12]. The conversion of the vertical axis in the seismic data of the conventional domain from depth to vertical time or Riemannian creates a non-orthogonal Riemannian coordinate system[13], known as Riemannian domain, then wavefield extrapolation for isotropic and anisotropic media in the new coordinate frame can improve efficiency in comparison with to Cartesian domain extrapolation results. The aims of this research are to improve the projection efficiency of the LSRTM processed data by using a finite difference scheme projected on a tau-mesh instead of a regular Cartesian one, to minimize calculation time, oversampling of the velocity wavefield, produce better imaging results with clearer structures, higher signal to noise ratio (S/N), higher resolution, more balanced and preserved amplitude, removing migration artefacts and diffracted noises which is caused by the surface topography.

Recent advancements, following the introduction of physics-informed neural networks by Raissi et al. (2019), have integrated deep learning and machine learning for seismic wavefield computation and its application in RTM, LSRTM, and FWI[14–17]. Neural networks (NN) are trained on random spatial input points and variations of the Helmholtz equation to calculate the scattered wavefield, using these computations as the loss function to refine network parameters for high-dimensional wavefield solutions. This machine-learning approach, constrained by the Helmholtz equation, is specifically chosen for solving the wave equation in seismic imaging. The network size is primarily influenced by the complexity of the desired wavefield, which increases with higher frequencies and more intricate models[16].

The vertical time axis -pseudodepth domain (τ) is the vertical axis for timemigration. It is defined as the two-way traveltime measured by a coinciding source and receiver on the surface. However, its originated from the Riemannian coordinates system (ξ_1,ξ_2,ξ_3). To test this transformation, we provide results and compare them with their corresponding ones in the Cartesian coordinates. LSRTM in the Riemannian domain for the one way-wave equation can be achieved by converting the velocity field from the cartesian to Riemannian domains and then calculating the wavefield in the latter domain.

Considering massive computation requirements of applying LSRTM, specifically for anisotropic media via either elastic or acoustic wave equations not to forget to mention its difficulty in application to industry, LSRTM in the Riemannian domain was introduced[13,18] to increase the efficiency of conventional LSRTM. On the other hand, Metallinos et al.[19] enhanced the modeling of the waves based on an existing sophisticated Boussinesq-type wave model. This model is exclusively being used in wave basins and complex coastal areas. This solution somehow similar to the main theme of applying pseudodepth domain conversion on seismic velocity for wave modelling. Yet the current research investigates the finite-difference operator conditions to stabilize and optimize the Riemannian wavefield propagation. And thus, that these conditions can be generalized to LSRTM algorithms, since the Riemannian wavefield, can be unstable and severely affects the migrated image when applying it. Additionally, this investigation can be generalized into new seismic acquisition methods that generates a wavefield, such as Marine vibrators[20,21]. The paper is divided as follow, first we introduce the affiliated wave equation used in LSRTM methods, then we highlight the conversion to Riemannian domain and the its wavefield extrapolator. In addition, we focus on the stability analysis of the numerical operator and finally we show our outcomes as a stabilized wavefield for two different types of underground models.

II. NUMERICAL SIMULATIONS OF LSRTM-WAVE EQUATION

LSRTM imaging now is a highly-matured depth-migration approach that applies both; Reverse-Time Migration and conjugate gradient algorithm to minimize the misfit function between Born modelled and original migration velocity models. Solving the wave equation to obtain wavefield solutions is an extremely important step in illuminating the earth subsurface using seismic imaging and waveform inversion methods and kernels. A number of techniques have been proposed to extend the classical Yee's (1966) finite-difference time-domain (FDTD) algorithm to a grid that is conformal to curved objects.

A. LSRTM Basic Theory

The scalar wave equation, commonly utilized in seismic wavefield computations within the Cartesian coordinate system, can be formulated as follows:

$$\frac{1}{v(x)^2}\frac{\partial^2 p(x,t)}{\partial t^2} - \nabla^2 p(x,t) = -\delta(x-x_s)s(t), \qquad (1)$$

where $p(x,t)$ is the acoustic wavefield, $\delta p(x,t)$ is the perturbation wavefield, and the background wavefield is $p_0(x,t)$. By inserting $m(x) = \{2\delta v/v_0(x)\}$ as a ReverseTime Migration reflectivity model, then the modeling operator for perturbation wavefield can be written in time-space domain backward as:

$$\frac{1}{v_0(x)^2}\frac{\partial^2 \delta p(x,t)}{\partial t^2} - \nabla^2 \delta p(x,t) = \frac{m(x)}{v_0(x)^2}\frac{\partial^2 p_0(x,t)}{\partial t^2}. \qquad (2)$$

Equation (1) is the equation used in RTM via Finite Difference Time-Domain scheme to generate the synthetic data, while Equation (2) is used in LSRTM to update the final image, since it has a reflectivity term $m(x)$, iteratively. Equation (1) represents the Reverse-Time Migration (RTM) imaging equation in a non-matrix form, incorporating the inverse of the Hessian matrix. The Hessian matrix, or simply the Hessian, is a square matrix consisting of second-order partial derivatives of a scalarvalued function or scalar field, which describes the local curvature of a function involving multiple variables. Solving for the inverse of the Hessian matrix directly is nearly infeasible due to the substantial computational and memory requirements, especially for both 2D and 3D seismic data. The objective is to determine a slowness perturbation that fits the input data by minimizing the misfit functional, as seen in methods like Multi-Source Least-Squares Reverse-Time Migration[7], by employing the forward (de-migration) operator L together with adjoint (migration) operator L^T, then the idea of the problem solution is to minimize the misfit between modeled data L_m and observed data d with conjugate gradient method, thus the solution to our problem is expressed as:

$$f(m) = \frac{1}{2}\|Lm - d\|^2 + \frac{\gamma}{2}\|m\|^2, \qquad (3)$$

For LSRTM, considered as a linearized inversion problem, the step length can be computed numerically as follows:

$$g^{(k+1)} = \left\{L^T\left[\mathrm{Lm}^{(k)} - d\right] + rm^{(k)}\right\}, \qquad (4)$$

$$\beta = \left\{\left(g^{(k+1)}\right)^T P g^{(k+1)}\right\} / \left\{\left(g^{(k)}\right)^T P g^{(k)}\right\}, \qquad (5)$$

$$z^{(k+1)} = \left\{Pg^{(k+1)} + \beta z^{(k)}\right\}, \qquad (6)$$

$$\alpha = \left\{\left(z^{(k+1)}\right)^T g^{(k+1)}\right\} / \left\{\left(Lz^{(k+1)}\right)^T Lz^{(k+1)}\right\}, \qquad (7)$$

$$m^{(k+1)} = \left\{m^{(k)} - \alpha z^{(k+1)}\right\} \qquad (8)$$

where r is the damping coefficient, g is the gradient of misfit function.

B. Conversion to Riemannian Coordinate System

A conventional seismic section consists of two axes: a horizontal axis representing distance and a vertical axis representing time. The vertical time axis, denoted as τ, is used for time migration[6,13,14,18,22–24]. It represents the two-way travel time measured when the source and receiver coincide on the surface, applicable in conventional time imaging for laterally invariant media. To transform a Cartesian point (x,y,z) to a vertical-time point with coordinates ($\xi 1, \xi 2, \xi 3$) the vertical axis must be converted to the time axis (τ) using the following relationship:

$$\tau_{TW} = 2\int_0^z \frac{dz'}{v(z')}, \qquad (9)$$

The inverse mapping is also straightforward, from differentiation of inverse functions, it follows:

$$z(x,y,\tau) = \int_0^z \left\{vm\left(x,y,\tau'\right)\right\} d\tau', \qquad (10)$$

and the two coordinate systems are related by:

$$\xi_1 = x_1, \xi_2 = x_2, \xi_3 = \tau(x,y,z) = \int_0^{x_3} \frac{dx_3'}{vm\,(x,y,z')}, \quad (11)$$

Leveraging the aforementioned transformation, we can interpolate seismic-space functions between Cartesian and Riemannian domains. This new system is a dynamically changing coordinate framework known as ray coordinates[14]. The mapping function for these coordinates can be efficiently calculated through ray tracing or Huygens wavefront tracing methods. In the context of defining the Laplacian operator for the previous acoustic wave equation in the Riemannian coordinate system,[23]define the associated metric tensor and its determinant as follows:

$$[g_{ij}] = \begin{pmatrix} E & F & 0 \\ F & G & 0 \\ 0 & 0 & \alpha^2 \end{pmatrix}, \quad (12)$$

where E,F,G and α^2 are deferential forms that can be found from mapping cartesian coordinates X to the Riemannian coordinates (ξ,η,ζ), as follows: $E = \{x\xi x\xi\}, F = \{x\xi x\eta\}, G = \{x\eta x\eta\}$ and $\alpha^2 = \{x\xi x\xi\}$.[11,14,18,24–26] have illustrated that the correlation between the Riemannian reference domain and its Cartesian equivalent is both unique and welldefined (i.e., one-to-one). This relationship can be established using a series of numerical mapping equations as follows:

$$xi = \{fi(\xi j)\}, \quad (13)$$

where i, j=1,2,3 . The elements of the matrix and are given through the relation:

$$[gij] = \left\{ \frac{\partial xk}{\partial \xi i} \cdot \frac{\partial xk}{\partial \xi j} \right\}, \quad (14)$$

The corresponding metric tensor is represented in matrix form as described by[14] and can be expressed as follows:

$$[g^{ij}] = \begin{pmatrix} G/J^2 & -F/J^2 & 0 \\ -F/J^2 & E/J^2 & 0 \\ 0 & 0 & 1/\alpha^2 \end{pmatrix}, \quad (15)$$

where J is the Riemannian domain geometrical spreading term and $J^2 = \{EG - F^2\}$. The finite-difference operator functions within this new coordinate framework, producing a distorted seismic wavefield. However, it is possible to achieve wavefield extrapolation in the Riemannian domain by incorporating a specific type of Gaussianlike wavelet. This method does not require altering the coordinate system and modifies the seismic data in a manner similar to traditional methods. Nonetheless, this approach requires further investigation to validate its effectiveness.

C. 1st-Order Riemannian Wavefield Extrapolator

On a Riemannian mesh the 3D acoustic monochromatic wave equation can be described as:

$$\Delta u = -\frac{\omega^2}{v_d^2} u, \quad (16)$$

where ω is temporal frequency, v_d is the spatially variable wave-propagation velocity of the medium and u is the wavefield. The Laplacian operator can be defined[18,23] as:

$$\Delta u = \sum_{i=1}^{3} \frac{1}{\sqrt{|g|}} \frac{\partial}{\partial \xi_i} \left(\sum_{j=1}^{3} g^{ij} \sqrt{|g|} \frac{\partial u}{\partial \xi_j} \right). \quad (17)$$

where g^{ij} is the associated metric tensor's component, $|g|$ is its determinant (Synge and Schild 1978).

The finite-difference operator of the 2-D acoustic wave equation for implementing reverse-time migration, which has only one converted axis in the Riemannian domain for isotropic media, as a system of second-order and first derivatives[13] is derived from the formula bellow:

$$\frac{\partial^2 P}{\partial t^2} = v_d^2 \left[\frac{\partial^2 P}{\partial x^2} + \frac{\partial^2 P}{\partial y^2} \right] + \frac{v^2}{v_m^2} \frac{\partial^2 P}{\partial \tau^2} - \frac{v^2}{v_m^2} \frac{\partial v_m}{\partial \tau} \frac{\partial P}{\partial \tau}. \quad (18)$$

where v_d is the medium P-wave velocity, v_m is mapping velocity, $\{\tau, z\}$ is the vertical time, P is the acoustic pressure/stress, u, wis particle momentum, σ is the slowness and as latter we will see in the stability analysis section. The final term on the left-hand side of the first equation in 18 influences only the amplitude of the extrapolated wavefield, and therefore, it can be disregarded during processing. Similarly, for anisotropic media as discussed by[27] , the 2-D wave equation in the 1st -order Riemannian domain's axis can be represented by the following second-order system of equations for horizontal and vertical stresses[24]:

where P_H, P_V is the horizontal and vertical stress, respectively, v_v is the vertical velocity in the direction of the axis of symmetry, η is an ellipticity $\left(\eta = \left\{\varepsilon - \frac{\delta}{1+2\delta}\right\}\right.$) and the NMO velocity is given from Thomsen parameters (ε, δ) as $v_d = \left\{v_v\sqrt{1+2\delta}\right\}$. In expression 19 we will only use the horizontal wavefield component P_H to perform finite-difference modelling. The coordinate transformation technique mentioned above enables the direct calculation of seismic wave propagation, cross-correlation, and inverse scattering imaging conditions in topographic coordinates. Subsequently, the resulting reverse-time migration images can be interpolated

$$
\begin{aligned}
\frac{\partial^2 P_H}{\partial t^2} &= \left\{(1+2\eta)v_d^2\left[\left(\frac{\partial}{\delta\xi_1}+\sigma_1\frac{\partial}{\partial\xi_3}\right)^2+\left(\frac{\partial}{\delta\xi_2}+\sigma_2\frac{\partial}{\partial\xi_3}\right)^2\right]P_H+\left(\frac{v_d v_v}{v_m}\frac{\partial}{\partial\xi_3}\right)\left(\frac{1}{v_m}\frac{\partial pv}{\partial\xi_3}\right)\right\}\\
\frac{\partial^2 p_V}{\partial t^2} &= \left\{v_d v_v\left[\left(\frac{\partial}{\delta\xi_1}+\sigma_1\frac{\partial}{\partial\xi_3}\right)^2+\left(\frac{\partial^2}{\delta\xi_2}+\sigma_2\frac{\partial^2}{\partial\xi_3}\right)^2\right]P_H+\left(\frac{v_v^2}{v_m}\frac{\partial}{\partial\xi_3}\right)\left(\frac{1}{v_m}\frac{\partial pv}{\partial\xi_3}\right)\right\}\\
\frac{\partial P}{\partial t} &= \frac{v^2}{v_m}\frac{\partial}{\partial x}(v_m * u)+\frac{v^2}{v_m}\frac{\partial}{\partial z}(v_m * w)\\
\frac{\partial u}{\partial t} &= \frac{\partial P}{\partial x}+\sigma * \frac{\partial P}{\partial z}\\
\frac{\partial w}{\partial t} &= \sigma * \frac{\partial P}{\partial x}+\left(\sigma^2+\frac{1}{v_m^2}\right) * \frac{\partial P}{\partial z},
\end{aligned}
\tag{19}
$$

back to the Cartesian domain using the inverse mapping function described in 10.

III. STABILITY AND CONVERGENCE ANALYSIS

The stability analysis ensures that the time step-size (Δt) is chosen such that the numerical solution remains stable and does not blow up. In this section we take another approach for transforming the governing partial differential equations of wave equation into a Riemannian manifold space and measure it analytical solution first though metric tensors and perform other stability tests to verify the conditions and constraints. Since measuring the stability aspects of the forward modelled pseudodepth domain-based wavefield is quite difficult due the tough nonlinearity nature of the governing equations.

From a discretization point of view, and due to the complexity of the 3-D and 2-D Riemannian domain wave equations, we simplified the calculations by taking the 1-D finite-difference solution as in Cartesian domain and defining an ansatz of Gaussian-like wavelet to investigate the stability and convergence conditions.

Assume that:

$$P_{tt} = {v_d}^2 P_{zz}, \tag{20}$$

where P_{tt} is the pressure wavefield-time derivative, P_{zz} is the pressure wavefield-spatial derivative and v_d is the medium velocity. When approximated by a finite-difference central formula we got:

$$\frac{P_i^{n+1}-2P_i^n+P_i^{n-1}}{\Delta t^2} = v_d^2\frac{P_{i+1}^n-2P_i^n+P_{i-1}^n}{\Delta z^2}. \tag{21}$$

Substitute the source term P_i^n with the unique matrix $p^n_{\exp(ikz_j)}$ where; $i=j=z=0,1,2,3\ldots$ are the time, spatial values and vertical spatial axis, respectively, k is the wavenumber, and the value $\exp(ikz_j)$ is called the vertical time. Expanding the solution in 23 as: where $CFL = \Delta t\frac{v_d}{\Delta z}$. The above equation represents the basic formula that can be implemented for numerical simulations, with the introduction of the vertical time term. A stability analysis with demonstration is given below.

$$
\begin{aligned}
\frac{P_i^{n+1}-2P^n_{\exp(ikz_j)}+u_i^{n-1}}{\Delta t^2} &= v_d^2\frac{P_{i+1}^n-2P^n_{\exp(ikz_j)}+P_{i-1}^n}{\Delta z^2}\\
u_i^{n+1}-2P^n_{\exp(ikz_j)}+P_i^{n-1} &= (CFL)^2\left[P_{i+1}^n-2P^n_{\exp(ikz_j)}+P_{i-1}^n\right]\\
u_i^{n+1} &= 2P^n_{\exp(ikz_j)}-P_i^{n-1}+(CFL)^2\left[P_{i+1}^n-2P^n_{\exp(ikz_j)}+P_{i-1}^n\right],
\end{aligned}
\tag{22}
$$

A. Courant-Friedrichs-Lewy (CFL) Stability Criterion

The Riemannian wave equation solution 23 that is under investigation with the scaling factor α, the CFL condition can be modified to account for the metric tensor and the scaling factor. The modified CFL condition for this specific scheme is a function of temporal-spatial and the wave velocity as: $\mathrm{CFL} = v_d * dt/(\alpha * dx) \leq 1$. Which can be achieved through the scaling factor α and in tuns its consequent yielded factor from the transformation between coordinate systems and the specific metric tensor matrix. From a practical point we can reshape the newly described CFL penalty conditions in the light of investigating the stability of the finite difference numerical solution and can be measured by rearranging 22 to yield:

$$p^2+\left(4\frac{v_d^2\Delta t^2}{\Delta z^2}\sin^2\left[\frac{k\Delta z}{2}-2\right]\right)P+1=0 \tag{23}$$

when $\beta = \left(4\frac{{v_d}^2\Delta t^2}{\Delta z^2}\sin^2\left[\frac{k\Delta z}{2}-2\right]\right)$ and P is the

amplification factor that depicts the growth of the wavenumber k, then to stabilize the propagation of the numerical solution it requires $|P| \leq 1$ for all possible values of the wavenumber k. It can be shown that, in order for the quadratic equation: $P^2 + \beta P + 1 = 0$, to have bounded roots satisfies $|P| \leq 1$, it is necessary that $|\beta| \leq 2$. This is equivalent to: $0 \leq \frac{{v_d}^2 \Delta t^2}{\Delta z^2} \sin^2 \frac{k\Delta z}{2} - 2 \leq 1$ for $\forall k$, which thus gives the same well-known Courant-Friedrichs-Lewy (CFL) condition (Courant et al., 1967; Mitchell, 1969; Liu and Sen, 2009; Kumar and Sharma, 2019) condition: $\Delta t \leq \frac{\Delta x}{v_d}$. From equation (18), after removing the last term in the right hand-side as it only affects the amplitude, the 1-D Riemannian wave equation associated central finite difference formula (20) can be re-written as:

$$P_{tt} = \frac{v_m^2}{v_d^2} U_{\tau\tau}$$

$$P_i^{n+1} = 2U^n_{\exp(ikz_j)} - P_i^{n-1} + (CFL)^2 \left[P^n_{i+1} - 2U^n_{\exp(ikz_j)} + P^n_{i-1} \right], \tag{24}$$

By comparison of the CFL conditions of $CFL = \Delta t \frac{v_m}{v_d \Delta \tau}$ and $CFL = \Delta t \frac{v_d}{\Delta z}$ we see that the mapping velocity is the controlling factor to stabilize the Riemanniar acoustic wavefield propagation. Where $U_{\tau\tau}$, in this case, is the 1^{st} order Riemannian axis special derivative which is called the vertical time axis measured in seconds, and v_m is the mapping velocity that projects the cartesian coordinates into the Riemannian counterparts. The mapping velocity in fact is measured from the Cartesian-basec original velocity model by using equations 910 and 11 and also it does not have a single value like in the conventional FDTD algorithm yet every depth layer has its own velocity bounded by a depth interval. When measuring the velocity analysis to extrac the picked velocities for stacking or migration, we can relate the subsurface medium velocities to the mapping velocity to depict the actual relationship as in the linear formula $v_m = \frac{CFL.\Delta\tau.v_d}{\Delta t}$ by applying proper time step-size on the finite difference operator. The vertical time term (τ) represents only a change of a variable from depth to vertical time and it is governed by the number of samples (n) as:

$$\Delta\tau \equiv \tau_{n+1} - \tau_n = \int_{z(\tau_n)}^{z(\tau_{n+1})} \frac{dz'}{v_m(x, y, z')}, \tag{25}$$

which corresponds to a fixed Riemannian domain sampling of the value $\Delta\tau$. This is that the effective sampling in depth, which is $z(\tau_{n+1}) - z(\tau n)$, increases with velocity. The sampling interval $\Delta\tau$ of the Riemannian-axis should be small enough to avoid wavefield aliasing when applying reverse-time migration wavefield's extrapolation in the Riemannian coordinate system as:which corresponds to a fixed Riemannian domain sampling of the value $\Delta\tau$. This is that the effective sampling in depth, which is $z(\tau_{n+1}) - z(\tau n)$, increases with velocity. The sampling interval $\Delta\tau$ of the Riemannian-axis should be small enough to avoid wavefield aliasing when applying reverse-time migration wavefield's extrapolation in the Riemannian coordinate system as:

$$\Delta\tau \leq \frac{v_{\min}}{10\,(f_{\max})}, \tag{26}$$

where $v_{\min}$ is the minimum velocity in the given seismic data velocity model and $f_{\max}$ is the maximum frequency of the finite difference operator. Usually, the mapping velocity is a slightly smoothed version of the true velocity model since equation 18 has a differential form of v_m. In addition, the spatial derivatives of the vertical-time for isotropic and anisotropic media equations (18 & 19) shall be approximated using Fourier pseudo-spectral methods to achieve the domain transformation, as:

$$\frac{\partial P}{\partial x_i} \approx F_i^{-1} \{ ik_i F_i \{P\} \}, \tag{27}$$

where the spatial F_i is the Fourier transform in the x_i direction and $i = 1$.

In practice, when processing field data, Fast Fourier Transform algorithm is preferred to be use instead of Fourier pseudo-spectral finite-difference methods as the latter is slower than the first. And then use its inverse FFT to convert back from frequency to time domain for the spatial derivatives of the Laplacian operator. The Fast Fourier Transform algorithm for approximating the spatial derivative(s) can be implemented in Frequency-Domain through:

$$\partial_x^\beta P = \text{IFFT} \left[(ik_x)^\beta \, FFT(P) \right], \tag{28}$$

while the time derivative can still be calculated in Time-Domain by:

$$\frac{\partial^2 P}{\partial t^2} = \frac{u(t + \Delta t) - 2P(t) + P(t - \Delta t)}{(\Delta t)^2} \tag{29}$$

after calculating the spatial derivative with FFT algorithm we must convert it back by inverse Fast Fourier Transform (IFFT) to continue with the conventional pure FiniteDifference Time-Domain scheme.

B. Sensitivity Assessment

The output wavefield of equation (24) is a complex-valued matrix meaning that the real part of it captures the actual pressure-wavefield displacements, and

the components of the wavefield that is 90 degrees out of the phase values, by the imaginary part. To demonstrate the sensitivity of this complex finite-difference discretization one approach is to visualize the real ($P_i^{n+1} = a + ib$), imaginary ($P_i^{n+1} = b$) parts or the magnitude $\left(abs\left(P_i^{n+1}\right) = \sqrt{a^2+b^2}\right)$, which provides insights into the strength and direction of the elements of the output matrix as in Figure 1 in isotropic medium. By

using Mur's absorbing boundary conditions in conventional space-time coordinates, the complex-valued wavefield propagates on 250×250 points with maximum 1^{st} -oder Riemannian axis length of 1.2 seconds through a one geological layer of 1500 m/s RMS velocity, and sampled by 1 ms . We see that for this wavefield the absorbingconventional coordinates boundary conditions did not absorb the waves as it supposed to be, hence a derivation of the boundary conditions must be obtained in the Riemannian domain to overcome this issue.

One way of understanding these insights gained from the numerical solutions in Figure 14, is to study the eigenvalues and eigenvectors of the complex-valued wavefield matrix P_i^{n+1} as:

$$\det\left(P_i^{n+1} - \lambda I\right) = \mathrm{v}, \tag{30}$$

where λ is eigenvalue-characteristic solutions, I is the identity matrix of the same dimension as matrix P_i^{n+1}. Each λ eigenvalue-characteristic solution has a non-zero associated eigenvector v satisfies:

$$\begin{aligned} &\left(P_i^{n+1} - \lambda I\right)\mathrm{v} = 0 \\ &\text{Or} \\ &\left(P_i^{n+1}\right)\mathrm{v} = \lambda \mathrm{v}, \end{aligned} \tag{31}$$

In Figure 2 which shows the outputs of both equations (30) & (31), the eigenvaluecharacteristic solution and its associated eigenvector is derived from the one-layer velocity model that is composed of 250 modes, where each eigenvalue corresponds to a mode of the matrix system, and each column in the eigenvector matrix represents the mode shape associated with its corresponding eigenvalue. Positive eigenvalues indicate a growth or less attenuation, while negative eigenvalues specify attenuation of the wave components. The magnitude of these values gives the rate of change. On the other hand, eigenvectors provide insights into the mode shapes or directions in the wavefield that are invariant under the propagation dynamics described by the operator, except for scaling. The complex nature of these vectors indicates that the wave components can undergo phase shifts and amplitude changes.

IV. SEISMIC EXAMPLES AND DISCUSSION

Figures 4, shows the solutions of the 1D wave equation of Sava and Fomel (2003) on different time-steps that is subjected with metric tensors and Riemannian skewed mesh for several forward time-steps with the choice of $\mathrm{CFL} = 0.1$ as penalty condition. We notice that, in addition to the wave speed in the medium (v_d) is subjected into another penalty conditions that is extremely crucial for the stability procedure which is the mapping velocity (v_m). The ratio between the medium speed and the mapping velocity is the main controlling factor in stabilizing this type of seismic wavefield through Finite-Difference modelling. The actual interpretation of these waveforms is that for greater time-steps the 1^{st} -order Riemannian axis modified FD scheme propagates the solution matrix in fewer time much faster the conventional FDTD counterpart. In comparison to the Riemannian-based wave equation in soliton theory by Majid et al. (2023) our analysis follows almost the same approach. The key step in this analysis of the present finite-difference solution in equation (24) is theelliptical source term $U^n_{\exp(ikz_j)}$. This term suggests an incorporation of a spatially varying characteristic into the wave equation, which is typically occurs in heterogeneous media or, in this case, on a 1^{st} -order Riemannian coordinate system where the metric tensors may vary with the position coordinates (i, j) and it gives the same results as in the Figure 4. This indicates that using this special source term of the ansatz source function can generate the wavefield in pseudodepth (1^{st} -order Riemannian domain) wave propagation in its conventional space-time as depicted in Figure 3.

Taking one subsurface layer with a unified anisotropic medium vertical velocity, with respect to the axis of the anisotropic, value of the order of 2 km/s (i.e., the medium is anisotropic and the value of the velocity is 2 km/s in all directions) and Normal Move-Out velocity of 1.643 km/s and anellipticity parameter η of 0.1 . As in Figures $5, 6, 7, 8\&9$ we notice that the Reverse-Time Migration (RTM) wavefield is not severely affected by changing the medium velocities as sampling rate remains fixed. The velocity model first incorporated numerically, then interpolated to Riemannian domain and finally applying the wavefield extrapolator on it to get the Riemannian wavefield.

From Figures 10 through 13 the isotropic Marmousi II velocity model has been converted into the 1^{st} -order Riemannian domain, with 501 samples on the vertical axis only by using an 8-point-triangle filter. We used a smoothed version of the Marmousi velocity as

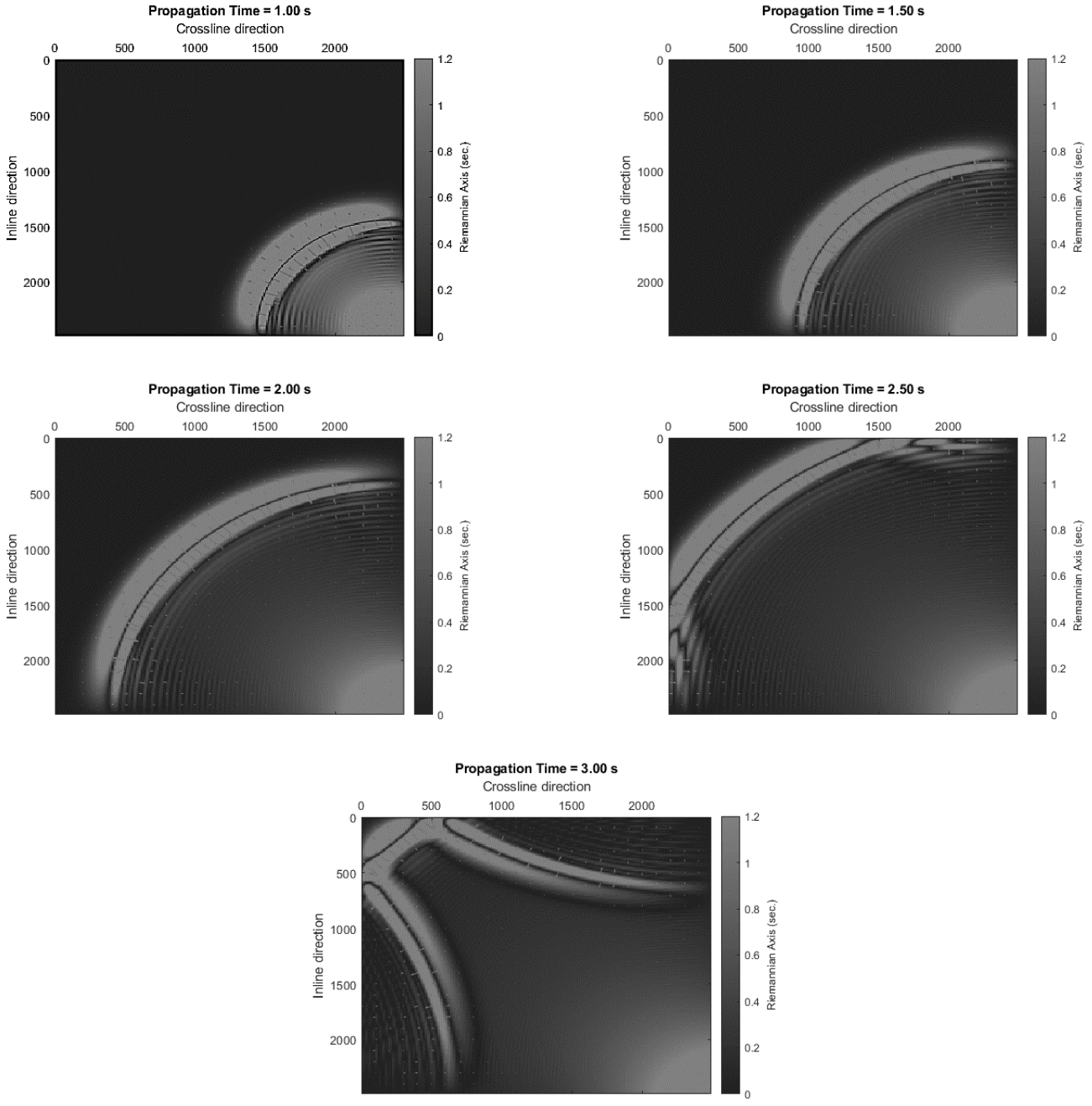

FIG. 1: Wavefield propagation snapshots at 1, 1.5, 2, 2.5, 3 seconds using the complex-valued 2D finite-difference operator in equation (24). Small arrows indicate the wavefield propagation direction.

the mapping velocity to compute the RTM wavefield in the Riemannian coordinate system. Again, this model shows rugged curvatures in the original velocity model which will cause many stability issues when applying the Riemannian-finite difference operator on it.

The famous Claerbout principle of reflector's position (1985) states that the reflector exists when the down-

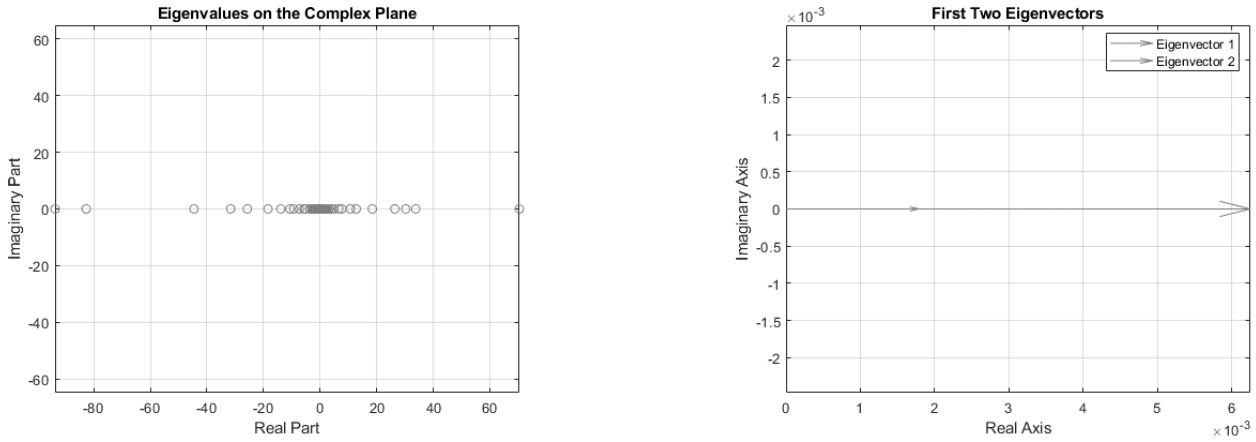

FIG. 2: Eigenvalue-characteristic solutions and associated eigenvectors of the finite-difference operators.

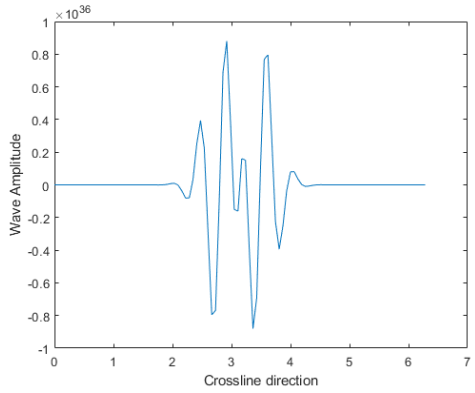

FIG. 3: 1D wavefield forward modeling generated using the source term of the finite-difference operator in equation (24) and applying the same conditions in Figure 4.

going and the up-going wavefields meet for both cases of the conventional and Riemannian wave equations. However, some un-stabilized propagation denoted as N1, N2 and N 3 zones noticed in Figure 13. Potential reasons behind these phenomena could be explained as a yielded form of the imperfect absorbing boundary conditions (in this case we use conventional space-time absorbing boundary conditions) which is specially derived to eliminate the reflected waves at the edge of the computation zone.

V. FIELD DATA TESTS

Another test (Figures 14 & 15) is done on a velocity model from a 2D land survey in Sudan, also interpolated and numerically solved in the Riemannian domain. The model has 20 m sampling interval and spreads to 20 km horizontally. Total depth is 8 km underground with a vertical sampling interval of 4 m . Sources are distributed all over the entire model with an interval of 40 m . The total seismic recording time is 5.00 s with a sampling interval of 5.00×10^{-3} s. A smoothed migration velocity model (Figure 14(b)) for 1^{st} -order Riemannian axis wavefield extrapolation is obtained, but slightly deformed when converted from the conventional space-time domain (Figure 14(a)), using the aforementioned mapping function (equation 9). Then the formulated finitedifference operator is applied to obtain the pre-stack LSRTM seismic wavefield (Figure15(a)) and the final pre-stack LSRTM image is depicted in Figure 15(b).

In Figure 15(a) the diffraction generated-waves were omitted after applying the proposed FDM approach and the common artificials were dismissed besides the seismic wavefield seems to be fairly stable. In addition, the migration result of the seismic section in Figure 15(b) is characterized by a significantly preserved amplitudes, which make the image very close to the true reflectivity model of the subsurface. Compared with the velocity model, the LSRTM image represents the geological structure sharply with a highly preserved amplitude, which is quite easy to interpret geologically.

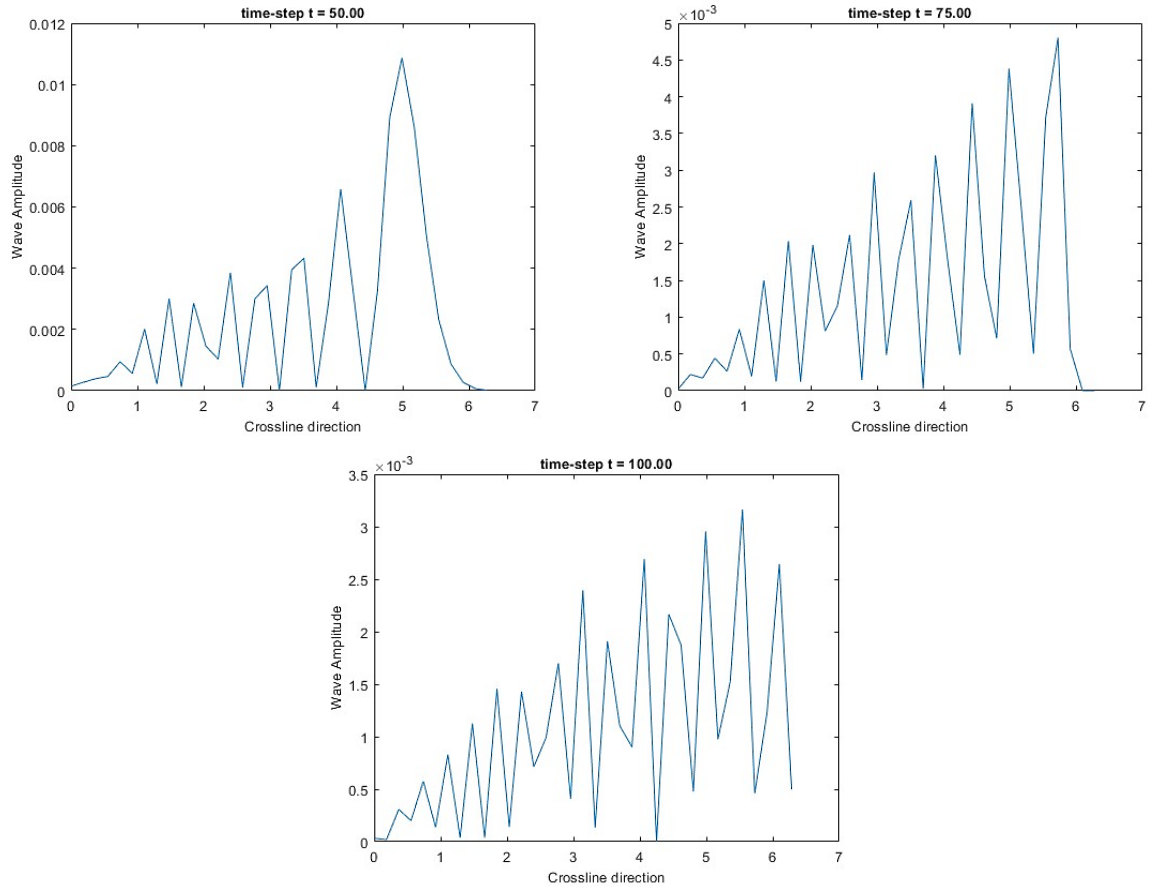

FIG. 4: Riemannian forward modeling solution of the 1D wave equation and its metric tensors in equation of Sava and Fomel (2005). (upper left) after 50 time-steps; (upper right) after 75 time-steps and (c) after 100 time-steps.

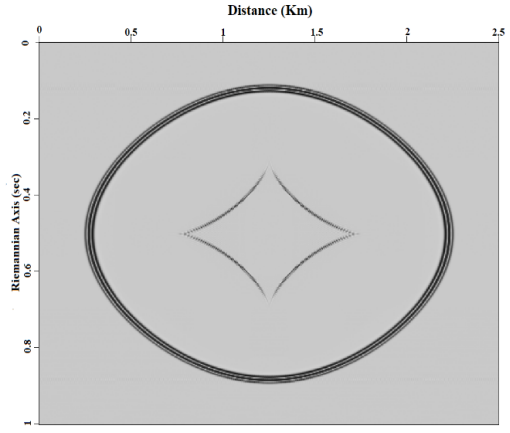

FIG. 5: Riemannian Reverse-Time Migration modelling impulse response of the velocity in Figure 4.

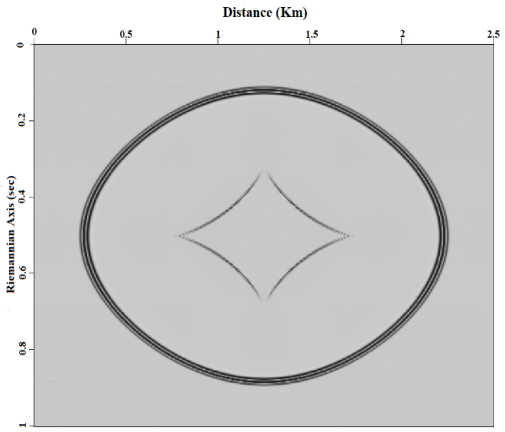

FIG. 6: Riemannian RTM response of medium velocity=2.5km/s with the same other anisotropic parameters.

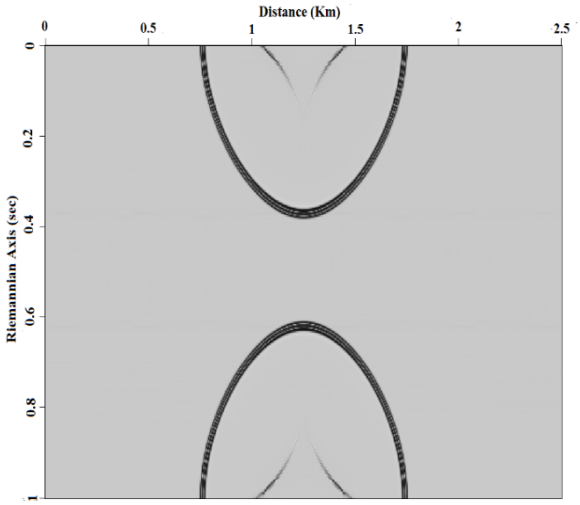

FIG. 8: Riemannian RTM response of medium velocity=1.5km/s with the same other anisotropic parameters.

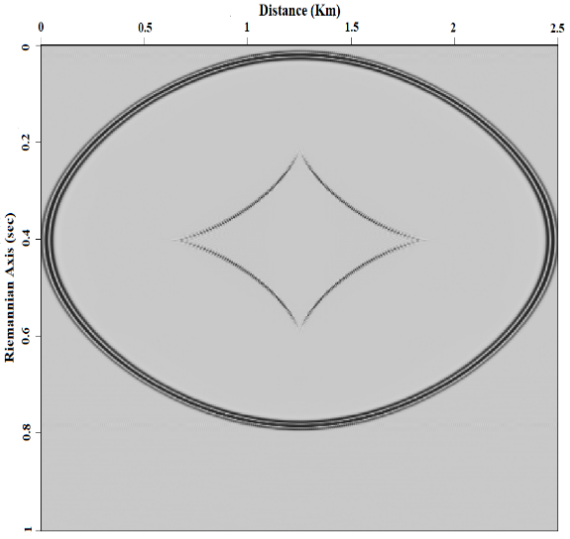

FIG. 7: Riemannian RTM response of medium velocity=1km/s with the same other anisotropic parameters.

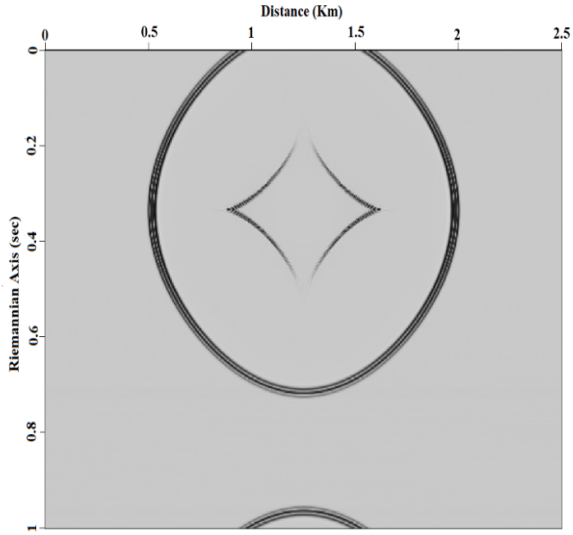

FIG. 9: Riemannian RTM response of medium velocity=3km/s with the same other anisotropic parameters.

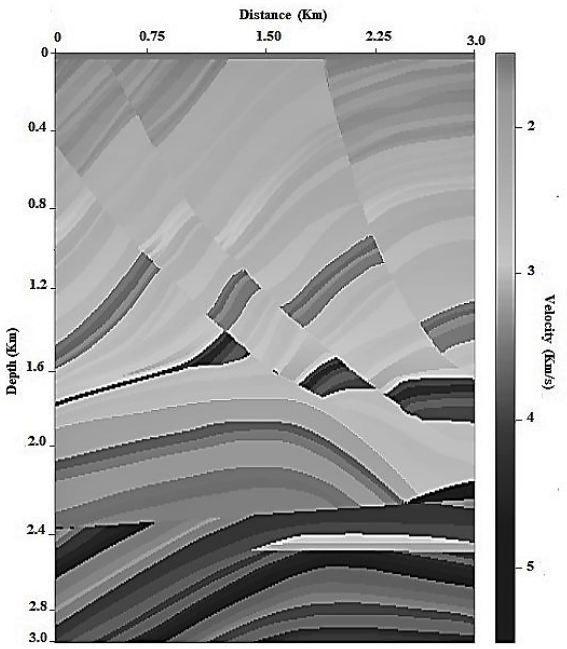

FIG. 10: Shallower part of Marmousi II velocity model.

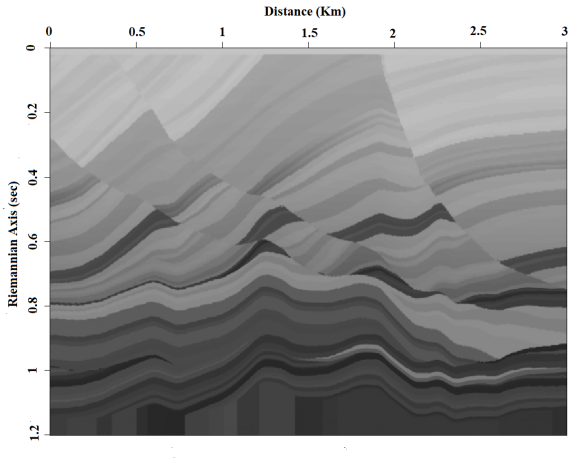

FIG. 11: The mapping velocity model interpolated to Riemannian domain with 501 samples by using 8-point-triangle filter strategy.

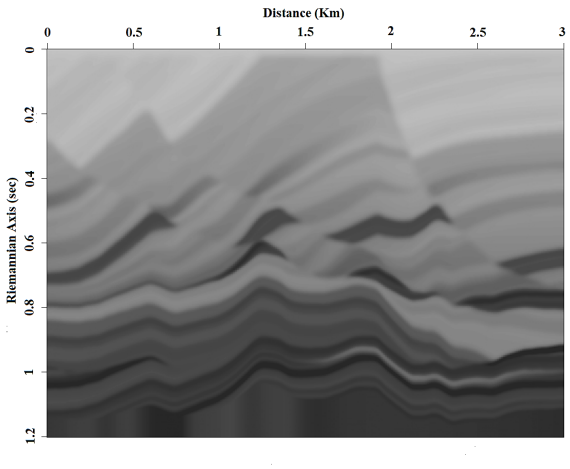

FIG. 12: A smoothed version of Fig.9 for finite-difference RTM modelling in Riemannian coordinates.

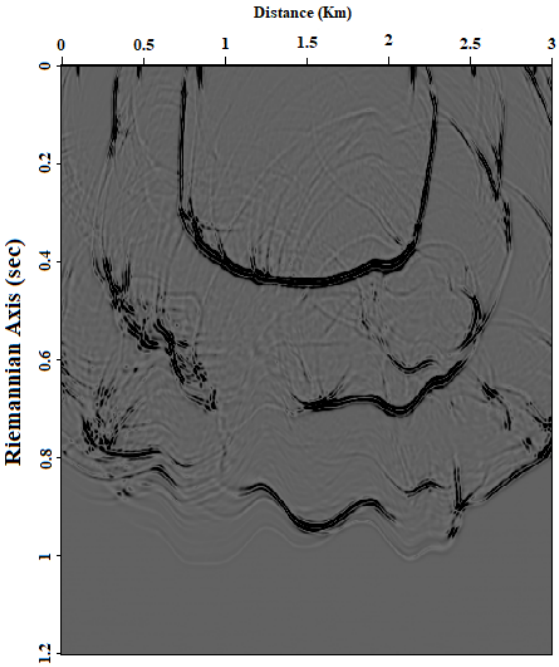

FIG. 13: Finite-Difference Riemannian forward modeling to extrapolate wavefield with indications to reflectors' position (Claerbout principle, 1985) of Figure 14.

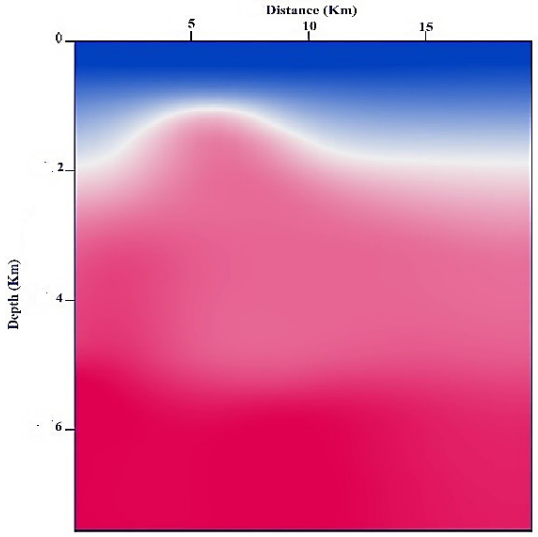

(a) Velocity model in Cartesian coordinate system.

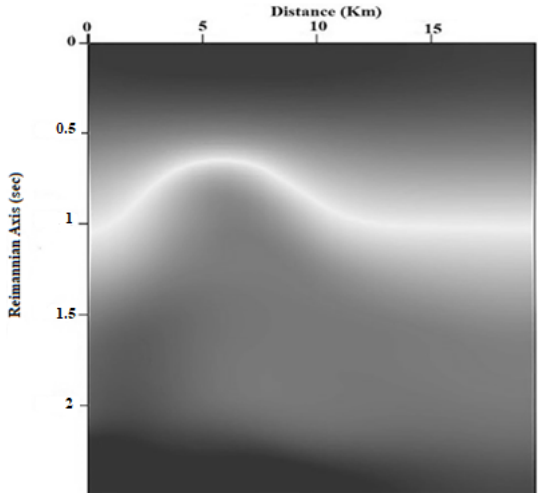

(b) Smoothed version in Riemannian domain.

FIG. 14: (a) Velocity model in the Cartesian coordinate system and a smoothed version of it in Riemannian domain (b).

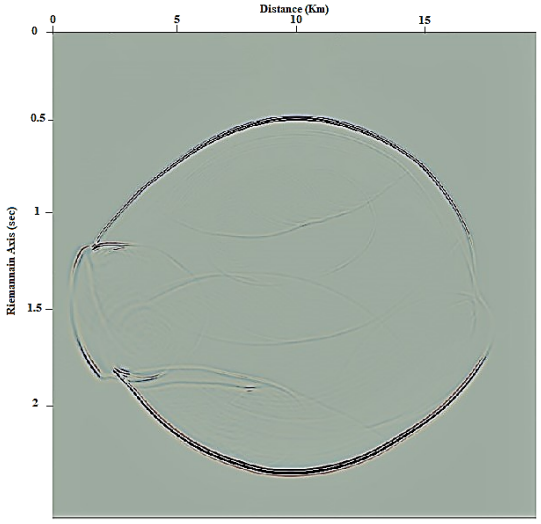

(a) Pre-stack wavefield extrapolation.

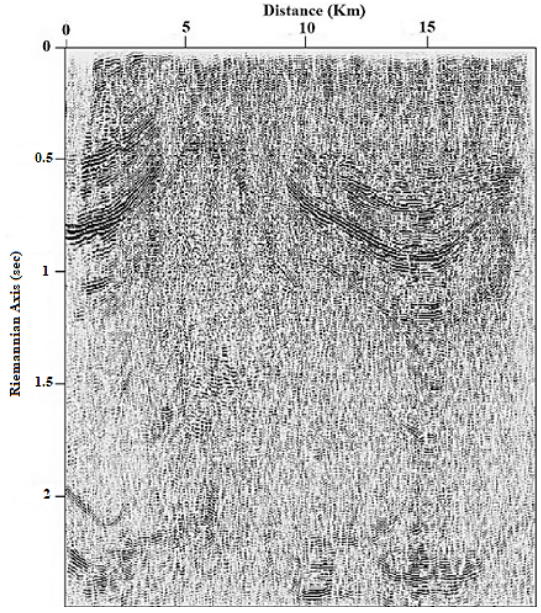

(b) Pre-stack LSRTM section.

FIG. 15: (a) Pre-stack wavefield extrapolation from field data in Figure 14(b) and its prestack LSRTM section (b) of the model constructed on.

CONCLUSION AND FINAL REMARKS

In this paper, we have analyzed the stability aspects of an alternative approach for LSRTM wavefield modelling in both isotropic and anisotropic media, suitable for least-squares reverse-time migration in Riemannian coordinate system. By using the same stability conditions for wavefield propagation in cartesian coordinate system and projecting a proper mapping velocity to initiate the reverse-time migration modelling in the Riemannian domain, wavefield extrapolation becomes more stable. The spatial differential derivative of the finite difference operator of this Riemannian wave equation is written entirely in terms of Fourier pseudo-spectral forms to solve the ansatz source term. We can describe the extrapolated Riemannian wavefield as water waves and its migrated image as loosed depth image. The stability requirements for reducing artefacts and finite difference operator errors could be used for construction of other methods and FDTD analysis. Furthermore, the derivation of the associated Riemannian-1D-wave equation sounds to be equivalent to the conversion of the same equation spatial operator into pseudodepth domain. Eigenvalues and eigenvectors analysis of the weighted finite-difference solution and the stability analysis show stability in wave modes and phase which support. This study can be extended for the elastic wave propagation in general, besides investigating the types of the source term that is used to initiate elastic seismic waves propagation and can be generalized for other type of partial differential equations involve in the study of shock waves.

ACKNOWLEDGMENTS

The authors are thankful for the fund for this research raised by the National Natural Science Foundation of China (41574098 & 41630964) and Major Scientific and Technological Projects of CNPC (ZD2019-183-003). And also, are thankful for the reviewer comments, as they were very constructive in increasing the quality of the paper. We thank students and research fellows within the SWPI laboratory at China University of Petroleum (Huadong) for their weekly fruitful discussion.

DECLARATION OF COMPETING INTEREST

The authors declare that they have no known competing commercial benefits or personal interconnections that could have appeared to influence the findings in this article.

REFERENCES

[1] G. Yao and H. Jakubowicz, "Least-squares reverse-time migration in a matrix-based formulation," Geophysical Prospecting **64**, 611–621 (2016).
[2] Y. Wang, W. Liang, Z. Nashed, X. Li, G. Liang, and C. Yang, "Seismic modeling by optimizing regularized staggered-grid finite difference operators using a time-space-domain dispersion-relationship preserving method," Geophysics **79**, T277–T285 (2014).
[3] P. C. Sava and S. Fomel, "Angle-domain common-image gathers by wavefield continuation methods," Geophysics **68**, 1065–1074 (2003).
[4] Y. Zhang, J. Sun, and S. Gray, "Reverse-time migration: amplitude and implementation issues," in *77th Annual International Meeting, SEG, Expanded Abstracts* (2007) pp. 2145–2149.
[5] S. Xu, Y. Zhang, and B. Tang, "3D angle gathers from reverse time migration," Geophysics **76**, S77–S92 (2011).
[6] J. Claerbout and S. Doherty, "Downward continuation of move-out corrected seismograms," Geophysics **37**, 741–768 (1972).
[7] W. Dai, P. Fowler, and G. T. Schuster, "Multi-source least-squares reverse time migration," Geophysical Prospecting **60**, 681–695 (2012).
[8] G. Yao, *Least-Squares Reverse-Time Migration*, Ph.D. thesis, Imperial College London (2013).
[9] H. H. Jaramillo and N. Bleistein, "The link of Kirchhoff migration and demigration to Kirchhoff and Born modeling," Geophysics **64**, 1793–1805 (1999).
[10] N. Bleistein, Y. Zhang, S. Xu, G. Zhang, and S. H. Gray, "Migration/inversion: think image point coordinates, process in acquisition surface coordinates," Inverse Problems **21**, 1715–1744 (2005).
[11] H. Khaniani, J. C. Bancroft, and E. von Lunen, "Iterative multiparameter waveform inversion of precritical reflection data using pre-stack time Kirchhoff approximation," Geophysics **81**, R15–R27 (2016).
[12] H. Sethi, J. Shragge, and I. Tsvankin, "Tensorial elastodynamics for coupled acoustic/elastic anisotropic media: incorporating bathymetry," Geophysical Journal International **228**, 999–1014 (2022).
[13] X. X. Ma and T. Alkhalifah, "Wavefield extrapolation in pseudodepth domain," Geophysics **78**, S81–S91 (2013).
[14] C. Song, T. Alkhalifah, and U. B. Waheed, "A versatile framework to solve the Helmholtz equation using physics-informed neural networks," Geophysical Journal International **228**, 1750–1762 (2021).
[15] T. Alkhalifah, C. Song, U. bin Waheed, and Q. Hao, "Wavefield solutions from machine learned functions constrained by the Helmholtz equation," Artificial Intelligence in Geosciences **2**, 11–19 (2021).
[16] H. Alzahrani and J. Shragge, "Seismic velocity model building using neural networks: Training data design and learning generalization," Geophysics **87**, 1–73 (2021).
[17] Y. Li, A. Bakulin, P. Nivlet, R. Smith, and T. Alkhalifah, "Target-oriented time-lapse elastic full-waveform inversion assisted by deep learning with prior information," in *SEG/AAPG/SEPM First International Meeting for Applied Geoscience & Energy* (2021).
[18] J. C. Shragge, "Riemannian wavefield extrapolation: Nonorthogonal coordinate systems," Geophysics **73**, T11–T21 (2008).

[19]A. Metallinos, M. Chondros, and A. Papadimitriou, "Simulating nearshore wave processes utilizing an enhanced Boussinesq-type model," Modelling **2**, 686–705 (2021).
[20]K. Almuteri, J. Shragge, and P. Sava, "Modeling the seismic wavefield of moving marine vibrator source," Geophysics **89**, 1–68 (2023).
[21]X. Li, G. Ji, B. Guan, Z. Du, C. Han, and Q. Cheng, "Elimination of seismic characteristics of solid-filled in ultra-deep fractured-vuggy reservoirs," Exploration Geophysics , 1–17 (2024).
[22]O. Yilmaz, *Seismic Data Analysis: Processing, Inversion, and Interpretation of Seismic Data* (SEG, 2001).
[23]P. Sava and S. Fomel, "Riemannian wavefield extrapolation," Geophysics **70**, T45–T56 (2005).
[24]A. Khalil, J. Sun, Y. Zhang, and G. Poole, "RTM noise attenuation and image enhancement using time-shift gathers," in *83rd Annual International Meeting, SEG, Expanded Abstracts* (2013).
[25]T. Alkhalifah, "Seismic data processing in vertically inhomogeneous TI media," Geophysics **62**, 662–675 (1997).
[26]H. R. Quiceno and C. Arias, "Analysis of the stability and dispersion for a Riemannian acoustic wave equation," Applied Mathematics and Computation **341**, 288–300 (2019).
[27]E. Duveneck, P. Milcik, P. M. Bakker, and C. Perkins, "Acoustic VTI wave equations and their application for anisotropic reverse-time migration," in *SEG Technical Program Expanded Abstracts 2008* (Society of Exploration Geophysicists, 2008) pp. 2186–2190.
[28]T. Alkhalifah, S. Fomel, and B. Biondi, "The space–time domain: theory and modelling for anisotropic media," Geophysical Journal International **144**, 105–113 (2001).
[29]T. Alkhalifah, C. Song, and X. Huang, "High-dimensional wavefield solutions based on neural network functions," in *First International Meeting for Applied Geoscience & Energy* (Society of Exploration Geophysicists, 2021) pp. 2440–2444.
[30]J. M. Carcione, G. C. Herman, and A. P. E. Ten Kroode, "Seismic modeling," Geophysics **67**, 1304–1325 (2002).
[31]J. F. Claerbout, "Toward a unified theory of reflector mapping," Geophysics **36**, 467–481 (1971).
[32]J. F. Claerbout, *Imaging the Earth's Interior* (Blackwell Scientific Publications, 1985).
[33]W. Dai and G. T. Schuster, "Plane-wave least-squares reverse-time migration," Geophysics **78**, S165–S177 (2013).
[34]T. De Jonge, V. Vinje, G. Poole, S. Hou, and E. Iversen, "Debubbling seismic data using a generalized neural network," Geophysics **87**, V1–V14 (2022).
[35]J. Virieux, "SH-wave propagation in heterogeneous media: Velocity-stress finite-difference method," Geophysics **49**, 1933–1942 (1984).
[36]J. Virieux, "P-SV wave propagation in heterogeneous media: Velocity-stress finite-difference method," Geophysics **51**, 889–901 (1986).
[37]J. Yang, Y. Liu, and L. Dong, "Least-squares reverse time migration in the presence of density variations," Geophysics **81**, S497–S509 (2016).
[38]A. Khalil, J. Sun, Y. Zhang, and G. Poole, "Domain limited solution of the wave equation in Riemannian coordinates," Geophysics **78**, T21–T27 (2013).
[39]S. T. Kaplan, P. S. Routh, and M. D. Sacchi, "Derivation of forward and adjoint operators for least-squares shot-profile split-step migration," Geophysics **75**, S225–S235 (2010).
[40]R. Kumar and A. Sharma, "Absorbing boundary condition (ABC) and perfectly matched layer (PML) in numerical beam propagation: a comparison," Optical and Quantum Electronics **51**, 1–13 (2019).
[41]S. Z. Majid, W. A. Faridi, M. I. Asjad, M. Abd El-Rahman, and S. M. Eldin, "Explicit soliton structure formation for the Riemann wave equation and a sensitive demonstration," Fractal and Fractional **7**, 102 (2023).
[42]P. Moczo, J. Kristek, and M. Galis, *The Finite-Difference Modelling of Earthquake Motions: Waves and Ruptures* (Cambridge University Press, 2014).
[43]P. Moczo, J. Kristek, M. Galis, E. Chaljub, and V. Etienne, "3-D finite difference, finite-element, discontinuous-Galerkin and spectral-element schemes analyzed for their accuracy with respect to P-wave to S-wave speed ratio," Geophysical Journal International **187**, 1645–1667 (2011).
[44]P. Moczo, J. O. A. Robertsson, and L. Eisner, "The finite-difference time-domain method for modeling of seismic wave propagation," in *Advances in Geophysics*, Vol. 48 (2007) pp. 421–516.
[45]W. A. Mulder, "A numerically exact non-reflecting boundary condition applied to the acoustic Helmholtz equation," Geophysics **86**, T341–T351 (2021).
[46]D. Pasalic and R. McGarry, "Convolutional perfectly matched layer for isotropic and anisotropic acoustic wave equations," in *SEG Technical Program Expanded Abstracts* (2010) pp. 2925–2929.
[47]J. O. A. Robertsson, J. O. Blanch, and W. W. Symes, "Viscoelastic finite-difference modeling," Geophysics **59**, 1444–1456 (1994).
[48]P. Sava and S. Fomel, "3-D traveltime computation using Huygens wavefront tracing," Geophysics **66**, 883–889 (2001).
[49]G. B. Savioli, J. E. Santos, J. M. Carcione, and D. Gei, "A model for CO2 storage and seismic monitoring combining multiphase fluid flow and wave propagation simulators. the Sleipner-field case," Computational Geosciences **21**, 223–239 (2017).
[50]N. Tu and F. J. Herrmann, "Fast imaging with surface-related multiples by sparse inversion," Geophysical Journal International **201**, 304–317 (2015).
[51]D. Wu, G. Yao, J. Cao, and Y. Wang, "Least-squares RTM with L1 norm regularisation," Journal of Geophysics and Engineering **13**, 666–673 (2016).
[52]G. Yao and H. Jakubowicz, "Least-squares reverse-time migration," in *74th Conference and Exhibition, EAGE, Expanded Abstracts* (2012).
[53]G. Yao, N. V. da Silva, and D. Wu, "Forward modelling formulas for least-squares reverse-time migration," Exploration Geophysics **49**, 506–518 (2018).
[54]G. Yao, D. Wu, and H. A. Debens, "Adaptive finite difference for seismic wavefield modelling in acoustic media," Scientific Reports **6**, 30302 (2016).
[55]K. Yee, "Numerical solution of initial boundary value problems involving Maxwell's equations in isotropic media," IEEE Transactions on Antennas and Propagation **14**, 302–307 (1966).
[56]C. Zeng, S. Dong, J. Mao, and B. Wang, "Broadband least-squares reverse time migration for complex structure imaging," in *84th Annual International Meeting, SEG, Expanded Abstracts* (2014) pp. 3715–3719.
[57]Y. Zhang, L. Duan, and Y. Xie, "A stable and practical implementation of least-squares reverse time migration," Geophysics **80**, V23–V31 (2015).